A reply to the review comments for

Cloud response to co-condensation of water and organic vapors over the boreal forest

Liine Heikkinen[1,2], Daniel G. Partridge[3], Sara Blichner[1,2], Wei Huang[4], Rahul Ranjan[1,2], Paul Bowen[3], Emanuele Tovazzi[3], Tuukka Petäjä[4], Claudia Mohr[1,2], and Ilona Riipinen[1,2]

[1]Department of Environmental Science (ACES), Stockholm University, Stockholm, Sweden
[2]Bolin Centre for Climate Research, Stockholm University, Stockholm, Sweden
[3]Department of Mathematics and Statistics, Faculty of Environment, Science and Economy, University of Exeter, Exeter, United Kingdom
[4]Institute for Atmospheric and Earth System Research (INAR) / Physics, University of Helsinki, Helsinki, Finland

Correspondence to: Liine Heikkinen (liine.heikkinen@aces.su.se) and Ilona Riipinen (ilona.riipinen@aces.su.se)

Responses to review comments

We thank the reviewer for their valuable comments on the manuscript. In the following, the reviewer comments are written in **red** and our responses in **black**. The manuscript edits are shown with the *italic font*.

Another change (addition), not requested by the reviewer is made to the UKESM1 description (Sect. 2.4). The Section now includes more information about the model configuration (in terms of droplet activation and updraft velocities):

L503– L513 (manuscript with tracked changes):

"The version of UKESM1 used includes developments to the droplet activation scheme from Mulcahy et al. (2020) to facilitate more consistent comparisons against PARSEC-UFO. In the standard configuration of UKESM1, aerosol particles are activated into cloud droplets using the droplet activation parameterization of Abdul-Razzak and Ghan (2000). This was replaced with the scheme from Barahona et al. (2010), which has been shown to be more consistent when compared against an adiabatic cloud parcel model over a range of conditions (Simpson et al., 2014; Partridge et al., 2015). Furthermore, in the standard configuration of UKESM1, the droplet activation scheme uses the distribution of sub-grid variability of updraft velocities according to West et al. (2014) with updates as described in Mulcahy et al. (2018). To facilitate more consistent comparisons against PARSEC-UFO simulations that calculate droplet number using a single average updraft velocity, the single characteristic updraft velocity (Peng et al., 2005) was used to initialize the droplet activation scheme in UKESM1."

General comment

The authors have improved and clarified the description of the model setup and modelling procedure. Understanding the assumptions behind the model better I have some additional questions that should be addressed before publication.

Reply: We are pleased to know that the model setup and the modeling procedure are currently more understandable, and happy to address the new questions that arose.

1. **The new Fig. A.1 indicates a strong dependence on the initialization RH. This raises the question how the no co-condensation case is defined. Could you add a more explicit description of the procedure that was applied for this case?**

Reply: We have added a table to Appendix A describing the "sensitivity study" simulation setup.

Manuscript edits:

L950 – L956 (manuscript with tracked changes):

"The effect of the initialization relative humidity, organic mass accommodation coefficient (α_{org}) and vaporization enthalpy (ΔH_{VAP}) on the modelled CDNC enhancements due to co-condensation are investigated for three conditions (simulation IDs #13, #55 and #95, respectively; Table S.1). The three conditions were selected as they are representative of low, median and high ΔCDNC simulated during BAECC. Table A.1. describes the simulation setup for this sensitivity study."

Table A.1:

"Table A.1. *The simulation setup for studying the sensitivities of initialization RH organic mass accommodation coefficient (α_{org}) and vaporization enthalpy (ΔH_{VAP}) on ΔCDNC is shown. Three simulation IDs are selected from the BAECC campaign (#13, #55 and #95, respectively; Table S.1) and three simulation sets (for varying initialization RH, α_{org} and ΔH_{VAP}, respectively) are performed for each ID with and without co-condensation. The initial temperature, aerosol chemical composition and PNSD vary between the different IDs, and are taken from Table S.1. A fixed updraft velocity of 0.3 m s^{-1} is applied for all the different simulation IDs and simulation sets.* "

Set	Co-condensation	Initialization RH [%]	α_{org}	ΔH_{VAP} [kJ mol^{-1}]
1a	OFF	[60, 80, 90, 95, 99]	1	150
1b	ON	[60, 80, 90, 95, 99]	1	150
2a	OFF	90	[0, 0.2, 0.4, 0.6, 0.8. 1.0]	150
2b	ON	90	[0, 0.2, 0.4, 0.6, 0.8. 1.0]	150
3a	OFF	90	1	[80, 100, 120, 150, 200]
3b	ON	90	1	[80, 100, 120, 150, 200]

2. It became clearer now how the ammonium sulfate content was derived. Yet, the range of AS assumed present in the condensed phase (minimum, average, maximum) is not mentioned. These numbers should be added and compared with the measurement range of ammonium sulfate with ACSM.

Reply: We thank the reviewer for the comment. We have followed an ion pairing method around three scenarios:

- When $n_{ammonium} / n_{sulfate} < 1$
  $n_{SA} = n_{sulfate} - n_{ammonium}$
  $n_{ABS} = n_{ammonium}$
  $n_{AS} = 0$
  $n_{AN} = 0$
  $n_{ON} = n_{nitrate}$

- When $1 \leq n_{ammonium} / n_{sulfate}$ and $n_{ammonium} / n_{sulfate} < 2$
  $n_{SA} = 0$

$n_{ABS} = (2 - n_{ammonium} / n_{sulfate}) \times n_{sulfate}$
$n_{AS} = (n_{ammonium} / n_{sulfate} - 1) \times n_{sulfate}$
$n_{AN} = 0$
$n_{ON} = n_{nitrate}$

- When $\boldsymbol{n_{ammonium} / n_{sulfate} \geq 2}$
  $n_{SA} = 0$
  $n_{ABS} = 0$
  $n_{AS} = n_{sulfate}$
  $n_{AN} = \min (n_{ammonium} - 2 \times n_{sulfate}, n_{nitrate})$
  $n_{ON} = n_{nitrate} - n_{AN}$

where n_x is the number of moles per species x per volume of air (mol m^{-3}). The different species are ammonium, sulfate and nitrate from ACSM measurements (converted to mol m^{-3}), SA is sulfuric acid, ABS is ammonium bisulfate, AS is ammonium sulfate, AN is ammonium nitrate, and ON is organic nitrate. The ion pairing method follows that of Äijälä et al. (2017), and it is a modified version of the method introduced in (Gysel et al., 2007). While these ion pairing methods are simplifying the complex behavior and interactions taking place within aerosol particles/populations, we consider that this method is sufficient for evaluating how realistic the ammonium sulfate mass fractions (f_{AS}) used as PARSEC-UFO inputs are. As a reminder, it is assumed that $f_{AS} = 1 - f_{Org}$ for the PARSEC-UFO input.

The comparison between the ion pairing output and PARSEC-UFO input is shown in Fig, AR.1a, and the min, max and median values are now given in Table S.2 (see manuscript edits). We can see that the f_{AS} used as PARSEC-UFO input is much higher than what the ion pairing predicts. This is not surprising given that the particles at SMEAR II contain less ammonium than would be required to fully neutralize the aerosol particles based on ion balance (Heikkinen et al., 2020). If the aerosol particles were very acidic during the BAECC campaign (we have not performed calculations with thermodynamic models), the aerosol liquid water content could be expected to be higher under 90% RH (PARSEC-UFO initialization). Given that we already treat the particles as potentially more hygroscopic within PARSEC-UFO than the ambient measurements suggest for SMEAR II, we keep the assumption of ammonium sulfate in the simulations.

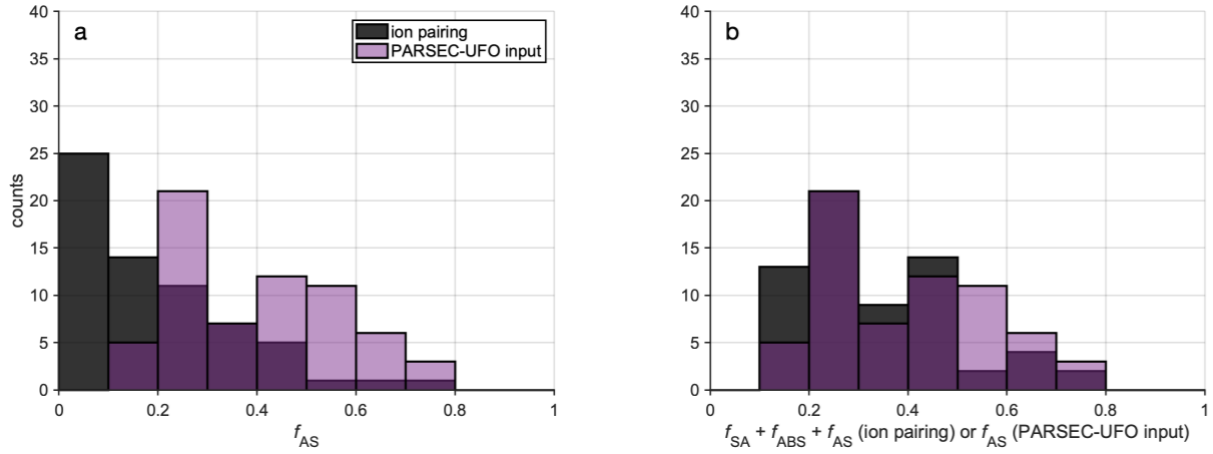

Figure AR.1 (a) Histograms depicting f_{AS} used as PARSEC-UFO input (in purple) and f_{AS} calculated using the ion pairing method (in black). **(b)** Histogram depicting f_{AS} used as PARSEC-UFO input (in purple) and the sum of f_{SA} + f_{ABS} + f_{AS} from the ion pairing (in black). The ion pairing calculations are not performed when the ammonium concentrations from the ACSM were negative. These cases are also excluded from the PARSEC-UFO input data for the comparison shown in this figure. This selection increases the median value f_{SA}, for example, and therefore these numbers should not be taken as representative values of f_{SA}, f_{ABS} or f_{AS} for the BAECC campaign.

Manuscript edits:

L301–L311 (manuscript version with tracked changes):

"The rest of the mass is assumed to be ***ammonium sulfate for the sake of simplicity, although an ion pairing method (Äijälä et al., 2017) would suggest significant contributions also from ammonium bisulfate (Table S.2).*** *For the simulations performed here, BC is not included given its small (about <5%) contribution to aerosol mass from late spring to summer (Luoma, 2021). While PARSEC-UFO does not utilize* κ*-Köhler theory (Petters and Kreidenweis, 2008), it might be useful to know that the assumed hygroscopicity, if translated to the hygroscopicity parameter* κ*, would be 0.14 and 0.72 for organics and ammonium sulfate, respectively (ideal solution; median* $\kappa_{tot} \approx 0.32$*). The assumed overall hygroscopicity is therefore likely to be overestimated, and it would exceed* κ *determined for SMEAR II experimentally in previous studies (e.g., Sihto et al., 2011 suggest* $\kappa = 0.18$*). Due to the likely overestimation of aerosol liquid water at initial conditions, it is also likely that the amount of organic vapor available for co-condensation after PARSEC-UFO initialization is underestimated "*

Table S.2:

"Table S.2 *Overview of ammonium sulfate mass fractions (f_{AS}) used in PARSEC-UFO simulations (first row), and the mass fractions obtained using an ion pairing method* (Äijälä et al., 2017 supplementary material)*. The mass fractions of sulfuric acid (f_{SA}), ammonium bisulfate (f_{ABS}) and ammonium nitrate (f_{AN}) are also provided. The ion pairing calculations are not performed when the ammonium concentrations from the ACSM were negative. These cases are also excluded from the PARSEC-UFO input data for the comparison displayed in this table. It is important to note that these numbers should not be taken as representative values of f_{SA}, f_{ABS} or f_{AS} for the BAECC campaign, because negative ammonium concentrations, which represent noise below the ammonium detection limit, are omitted. In addition, for more reliable estimates of the ion pairing, more sophisticated thermodynamic modeling is required."*

Method	Parameter	Min	Max	Median
$f_{AS} = 1 - f_{Org}$ [a]	f_{AS}	0.16	0.75	0.32
Ion pairing	f_{AS}	0	0.73	0.15
	f_{ABS}	0	0.52	0.12
	f_{SA}	0	0.26	0
	$f_{AS} + f_{ABS} + f_{SA}$	0.12	0.75	0.29
	f_{AN}	0	0.17	0

[a] *Used as PARSEC-UFO input.*

Table 1:

Table 1 *Overview of the PARSEC-UFO simulation input parameters that remain unchanged in all of the simulation sets conducted with or without co-condensation. The updraft velocities, organic volatility distributions and organic vapor concentrations that change between simulation sets are reported in Table 2 together with the median model outputs. The time series of these model input data are shown in Fig.1. All the modelling scenarios are initiated at 90% relative humidity.*

Parameter	Min	Max	Median
Aitken mode number conc. N_1 [cm^{-3}] [a]	160	12 316	1491

Accumulation mode number conc. N_2 [cm^{-3}] [a]	44	2 433	560
Aitken mode geometric mean dry diameter D_1 [nm] [a]	7.1	71.0	23.8
Accumulation mode geometric mean dry diameter D_2 [nm] [a]	62.6	201.9	115.3
Geom. standard deviation of Aitken mode σ_1 [a]	1.50	2.08	1.75
Geom. standard deviation of accumulation mode σ_2 [a]	1.33	2.06	1.75
Number of PNSD size bins	400	400	400
Organic mass fraction f_{Org} [%] [b]	25	84	68
Ammonium sulfate mass fraction f_{AS} [%] [c]	**16**	**75**	**32**
Initial T [K] [d]	271	295	279
Initial p [hPa]	980	980	980
Initial RH [%]	90	90	90
Mass accommodation coefficient α	1	1	1
Vaporization enthalpy for organics ΔH_{vap} [kJ mol^{-1}] [e]	150	150	150
Effective soluble fraction of organics	1	1	1
Surface tension γ [mN m^{-1}]	72.8	72.8	72.8

[a] *Retrieved from fits assigned onto the measured aerosol size distributions (Aalto et al., 2001) using a fitting algorithm by Hussein et al. (2005).*
[b] *Retrieved from aerosol chemical composition measurements (Heikkinen et al., 2020).*
[c] $f_{AS} = 1 - f_{Org}$
[d] *Retrieved from radio soundings (ARM Data Center, 2014). The temperatures shown were recorded when the relative humidity measured by the radiosonde reached 90%, i.e., the initial relative humidity used for the adiabatic ascents.*
[e] *Note that in the volatility distribution construction (offline from PARSEC) the ΔH_{vap} is adjusted following Epstein et al. (2010).*

3. Figure 4 shows that also the volatility bin $\log_{10}C^* = 7$ partitions partly to the condensed phase below cloud base. Is this realistic? Could you doublecheck this finding with a gas-particle equilibrium partitioning calculation at the RH just below cloud base?

Reply: We have calculated the equilibrium absorptive partitioning for three cases (simulation similar to IDs #55 and 83 in terms of the PNSD, and for a hypothetical condition similar to #83 except D_2 = 400 nm) using the multimodal approach introduced in Crooks et al. (2016). However, different to Crooks et al. (2016), the volatility distribution is changed from $\log_{10}C^*$ = [-6:1:3] to $\log_{10}C^*$ = [0:1:7].

The equilibrium partitioning does not predict any partitioning from the bin $\log_{10}C^* = 7$ to the condensed phase for simulation ID #55 (Fig. AR.2), while some is predicted for simulation ID #83 (Fig. AR.3).

If we significantly increase the diameter of the larger aerosol mode (D_2, represented as the mode median diameter in Crooks et al., 2016), a large fraction of the bin $\log_{10}C^* = 7$ partitions to the condensed phase (Fig. AR.4). This is in line with our finding stating that the fraction of organic vapor from bin $\log_{10}C^* = 7$ condensed below cloud base depends on the available surface area (condensation sink). This is shown in Fig. S.4, where more vapor from bin $\log_{10}C^* = 7$ partitions to the condensed phase when the s_{max} reached during the adiabatic ascent remains low (s_{max} relates to the condensation sink as shown in Eq. (3) in the manuscript main text). Note that the for simulation #83 $s_{max} \approx 0.12\%$, and for simulation #55 $s_{max} \approx 0.22\%$ when co-condensation is on.

We would like to further highlight, as also pointed out by Crooks et al. (2018), and heavily discussed in our work, that co-condensation is a *dynamic* phenomenon. The equilibrium absorptive partitioning at cloud base cannot therefore show the same result as shown in Figure 4 in the manuscript, because the time component is missing from the Crooks et al. (2016) equations. One could, of course, attempt to utilize the parameterization for *dynamic partitioning* introduced later by Crooks et al. (2018), but this would lead to the

evaluation whether the Crooks et al. (2018) parameterization actually works for the updated volatility distribution *x*-axis ($\log_{10}C^*$ = [-6:1:3] vs $\log_{10}C^*$ = [-0:1:7]) rather than evaluating whether the condensation of bin $\log_{10}C^*$ = 7 in PARSEC-UFO is realistic. That is why we did not continue on that path.

As we do not believe the equilibrium absorptive partitioning to represent co-condensation appropriately, and the condensation of the bin $\log_{10}C^*$ = 7 is assumed to be more realistically represented for this system by PARSEC-UFO (e.g., Figs. 4 and S.4), we refrain from showing figures AR.2–AR.4 with the manuscript. However, we hope our answer has satisfied the reviewer, and we thank for this question.

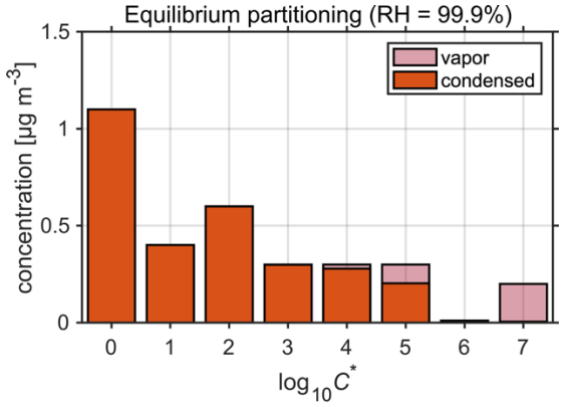

Figure AR.2 Equilibrium absorptive partitioning of organics between two aerosol modes as predicted using the Crooks et al. (2016) approach. The partitioning is calculated using the following input: T = 277 K (temperature), p = 957 hPa (pressure), RH = 99.9 % (relative humidity), f_{Org} = 0.7 (organic mass fraction), D_1 = 50 nm, D_2 = 95 nm (median diameters for modes 1–2), N_1 = 235 cm^{-3}, N_2 = 719 cm^{-3} (number concentrations for modes 1–2), σ_1 = σ_2 = 1.77 (geometric standard deviation for modes 1–2). The PNSD input is similar to simulation ID #55 (Table S.1).

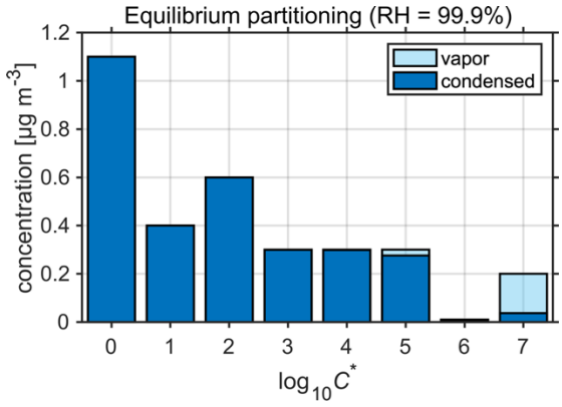

Figure AR.3 Equilibrium absorptive partitioning of organics between two aerosol modes as predicted using the Crooks et al. (2016) approach. The partitioning is calculated using the following input: T = 277 K (temperature), p = 957 hPa (pressure), RH = 99.9 % (relative humidity), f_{Org} = 0.76 (organic mass fraction), D_1 = 16 nm, D_2 = 139 nm (median diameters for modes 1–2), N_1 = 162 cm^{-3}, N_2 = 1823 cm^{-3} (number concentrations for modes 1–2), σ_1 = σ_2 = 1.6 (geometric standard deviation for modes 1–2). The PNSD input is similar to simulation ID #83 (Table S.1).

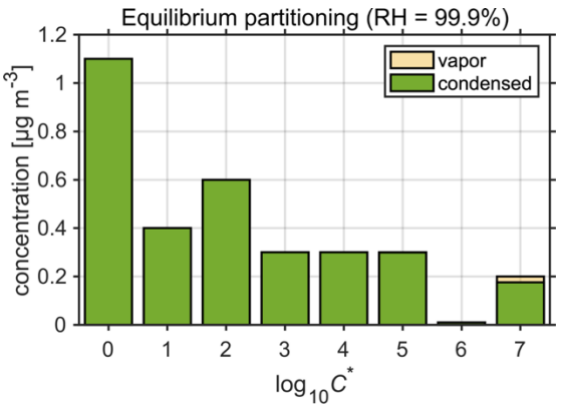

Figure AR.4 Equilibrium absorptive partitioning of organics between two aerosol modes as predicted using the Crooks et al. (2016) approach. The partitioning is calculated using the following input: T = 277 K (temperature), p = 957 hPa (pressure), RH = 99.9 % (relative humidity), f_{Org} = 0.76 (organic mass fraction), D_1 = 16 nm, ***D*₂ = 400 nm** (median diameters for modes 1–2), N_1 = 162 cm^{-3}, N_2 = 1823 cm^{-3} (number concentrations for modes 1–2), $\sigma_1 = \sigma_2$ = 1.6 (geometric standard deviation for modes 1–2). D_2, used as the equilibrium partitioning input, is increased compared case shown in Figure AR.3.

4. The examples of DMPS in Fig. S.1, which show a clear Hoppel minimum, seem to have a quite pronounced accumulation mode so that all droplets that activate should stem from this mode if one compares the average cloud droplet number concentrations and critical radius with the accumulation mode particle number concentration and mean dry diameter. If this were the case, it is unclear why the Hoppel minimum should be of relevance. To make the role of the Hoppel minimum clearer, it would be interesting to see a plot of the interstitial particle size distribution after activation for the cases with a Hoppel minimum.

Reply: We thank the reviewer for the question, as it provides an opportunity to clarify the importance of the PNSD shape on the modelled CDNC enhancements. We have prepared three figures for the supplementary material. Figures S.9 and S.10 show the initial dry PNSD and the smallest activated dry radii for the simulations gaining the ten highest and ten lowest CDNC enhancements, respectively. These figures reveal that in the case of PNSDs with Hoppel minima – associated with the lowest CDNC enhancements – the reduction in the smallest activated dry size occurs in the Hoppel minimum region (Figure S.10). This is not surprising, as the Hoppel minimum is typically located between ~80–100 nm, and minima are understood to result from cloud processing, therefore pinpointing the activation diameters in the real atmosphere. When looking at Figure S.9, with the nascent ultrafine particle modes, we can see that the smallest activated dry diameters are situated in the steep slopes on the nascent ultrafine particle modes. Based on these figures we can conclude that the sum of particles within the dry activation diameter reduction ranges are higher in Figure S.9 compared to Figure S.10. This results from

- the higher derivative of the PNSD slope within this range
- the larger smaller activated dry diameter reduction range window, and the higher number of particles

as these together lead to a larger sum of particles (the integral of the PNSD within the reduction range window) that can activate due to co-condensation in the latter.

Next, we show that the reduction in the smallest activated dry radii correlates with ΔCDNC well, when Hoppel minima are present in the initial PNSD (Fig. S.11a), and that a higher organic vapor concentration increases the modeled CDNC (Fig. S.11b). However, similar reductions in smallest activated dry diameters and organic vapor concentrations can lead to significantly higher CDNC enhancements in the presence of the nascent ultrafine particle modes compared to PNSD with a Hoppel minimum (Fig. S.11a).

Manuscript edits:

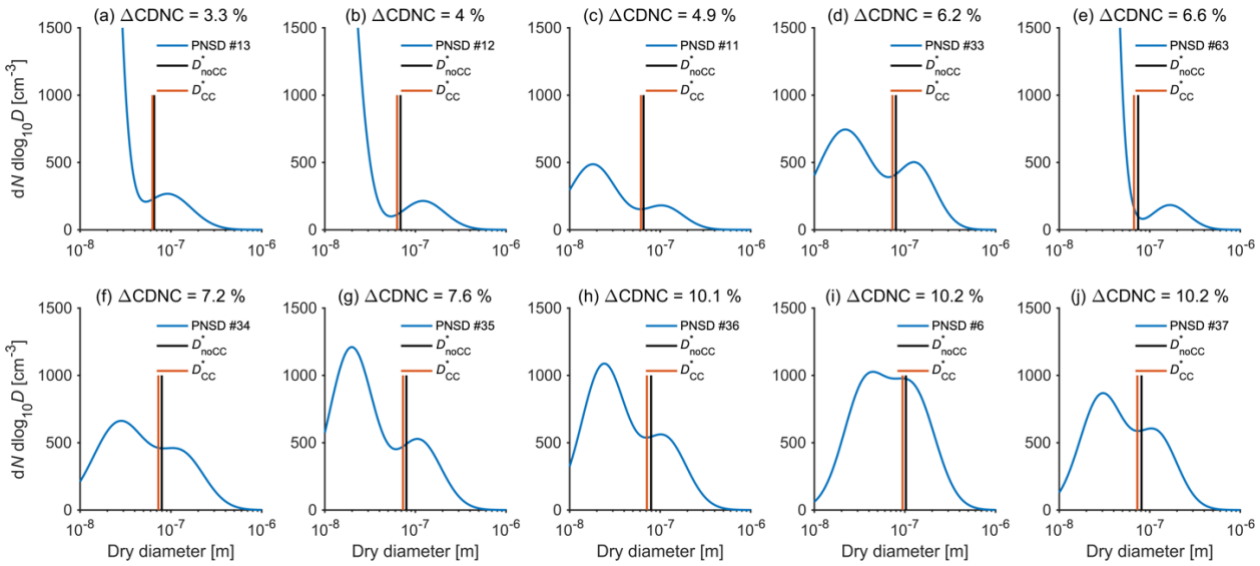

Figure S.10. *The different panels show the initial dry PNSD (in blue) for the 10 simulations yielding the lowest CDNC enhancements due to co-condensation. The smallest activated dry diameters for simulations without co-condensation (D^*_{noCC}) are highlighted with the black vertical lines, and the smallest activated dry diameters with co-condensation enabled (D^*_{CC}) are shown with the red/orange vertical lines.*

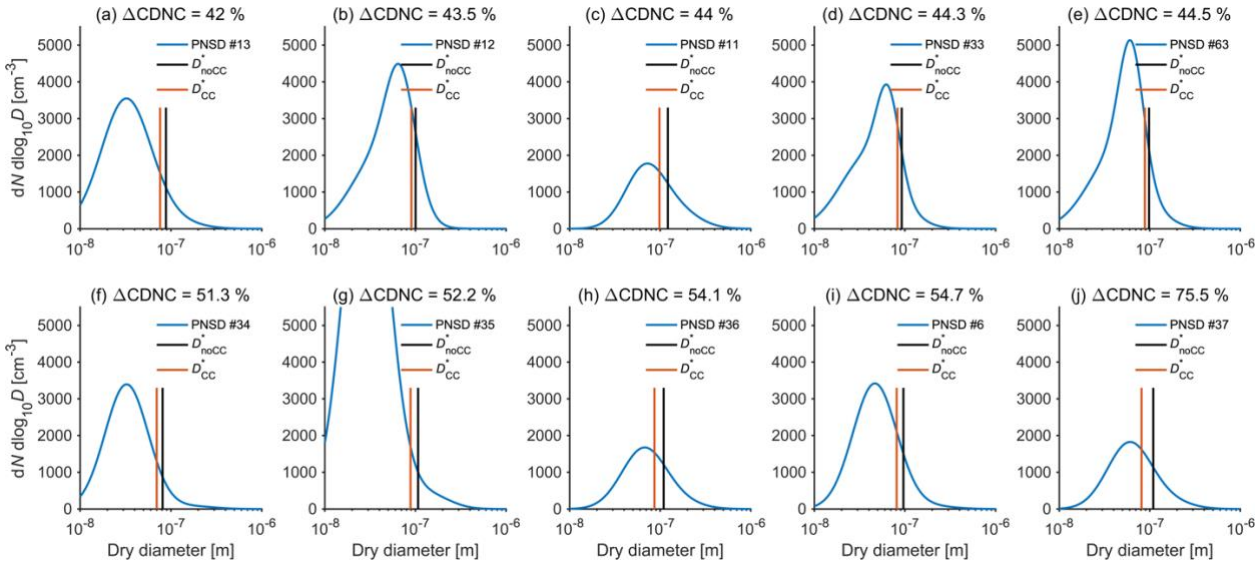

Figure S.9. *The different panels show the initial dry PNSD (in blue) for the 10 simulations yielding the highest CDNC enhancements due to co-condensation. The smallest activated dry diameters for simulations without co-condensation (D^*_{noCC}) are highlighted with the black vertical lines, and the smallest activated dry diameters with co-condensation enabled (D^*_{CC}) are shown with the red/orange vertical lines.*

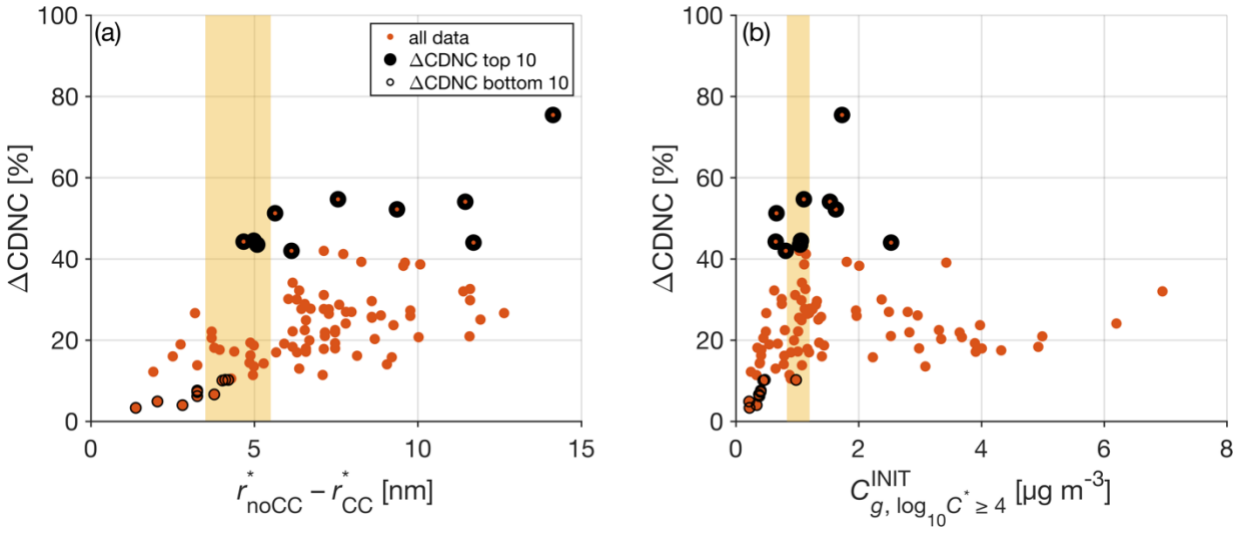

Figure S.11. (a) *The relationship between the modeled ΔCDNC and the reduction in the smallest activated dry radii. All the simulations are shown with the red/orange markers, and the top 10 ΔCDNC are highlighted with the thick black marker edges, and the bottom 10 ΔCDNC with the thin black edges.* ***(b)*** *The relationship between ΔCDNC and the initial organic vapor concentration within the $log_{10}C^*$ range from -4 to 4 ($C^{INIT}_{g,-4:4}$).* The ~similar ranges in the reduction of smallest activated dry radii, and $C^{INIT}_{g,-4:4}$ for the *bottom 10 ΔCDNC and the top 10 ΔCDNC are highlighted in yellow demonstrating the significantly different ΔCDNC resulting from the varying PNSD shapes between the two groups.*

L684–L707 (manuscript with tracked changes):

As briefly mentioned in the previous section, PNSD affects ΔCDNC along with the initial meteorological conditions. The importance of Aitken mode in ΔCDNC associated with turning co-condensation on in PARSEC-UFO is exemplified in Fig. 5b for the 0.3 m s^{-1} updraft simulations. In this figure, the initial dry PNSD are averaged from the simulations with the highest 25% and lowest 50% modelled ΔCDNC, respectively. The PNSD corresponding to the highest 25% of the modelled ΔCDNC has a very minor accumulation mode and a large Aitken mode (with respect to the mode total number concentrations i.e., N_2 and N_1, respectively) with a diameter (D_1) of ~40 nm (D_2 is ~110 nm). It is named as $PNSD_{NUM}$, where NUM refers to a strong nascent ultrafine mode characteristic of the shown size distribution. ***The $PNSD_{NUM}$ gain the highest ΔCDNC despite a relatively small change in the smallest activated dry radii, because of the steep PNSD slope in the size-range where the smallest activated dry radii reduce (Figure S.9; Sect. 3.2). The slope compensates for a comparatively small reduction in the smallest activated dry diameters by sharply increasing the number of particles that activate, when co-condensation is enabled.*** *The PNSD corresponding to the lowest 50% of the modelled ΔCDNC is strongly bimodal, where the Aitken and accumulation modes are almost equal in terms of N. Moreover, the two modes are separated by a clear Hoppel minimum (Hoppel and Frick, 1990). Hoppel minimum is characteristic for aerosol populations, which have undergone cloud processing.* ***The PNSD associated with the lowest ΔCDNC tend to have the smallest activated dry diameters close to the Hoppel minimum, where the PNSD slope is negligible (Figure S.10). Therefore, the integral through this range provides less particles to be activated to cloud droplets, and the ΔCDNC remain low. It should be noted, however, that the reductions in the smallest activated dry radii are on average higher in the simulations initialized with $PNSD_{NUM}$ (Figure S.11a) due to higher availability of organic vapors (Figure S.11b) and their condensation to a more critical size range.***

Nonetheless, it is evident that the shape of the PNSD dictates the magnitude of the ΔCDNC, as a ~4 nm reduction in the smallest activated dry radius can lead to a CDNC enhancement of ~45% in the case of a $PNSD_{NUM}$, while in the case of a PNSD with a Hoppel minimum, ΔCDNC would be only ~10%. *These results underline that environments rich in particles from a local source would be more susceptible to high ΔCDNC due to co-condensation while regions with aged and cloud processed size distributions are affected less (ΔCDNC<20% in our simulations; Fig. 5a).*

Specific and technical comments (lines refer to marked-up manuscript)

- **Line 43: the sentence is not complete.**

Reply: We thank the reviewer for noticing this. We have completed the sentence.

Manuscript edits:

L39–L41:

"For the critical aerosol size distribution regime, ΔCDNC ***is shown to be*** *sensitive to the concentrations of semi-volatile and some intermediate-volatility organic compounds (SVOCs and IVOCs) especially when the overall particle surface area is low."*

- **Lines 581–585: This text is not fully elaborated. "Below CB" is explained here twice in different words. Should the original version be deleted?**

Reply: We thank the reviewer, and see why the text was confusing. We have clarified the text and hope it is more understandable now.

Manuscript edits:

L547–L550:

"*Both SVOC and IVOC concentrations decrease significantly along the adiabatic ascent in subsaturated conditions below cloud base* ***(CB). Given that the PARSEC-UFO simulation output is saved with 2-meter vertical resolution, "below CB" contains all the simulation output under subsaturated conditions, and the RH at CB is defined as*** **min(RH ≥ 100 %)***."*

- **Line 663: "dry radii" instead of "dy radii".**

Reply: We thank the reviewer for spotting the typo. This is corrected in the manuscript.

- **Lines 687–689: Why should this be surprising? A major difference is introduced by scaling the volatility bin to lower temperature and the highest two volatility bins from Topping et al. are lost.**

Reply: We thank the reviewer and agree that this is not surprising at all. We have removed the "Perhaps surprisingly" from the sentence.

- **Figure 3: Panel labelling (a–e) is missing.**

Reply: We thank the reviewer. Labels (a–e) are now added to the figure.

- **Figure caption of Fig. 3: Why absolute change when the ratio s*cc/s*no-cc is plotted?**

Reply: We thank the reviewer for spotting this mistake. We have improved the description of the b-panel.

Manuscript edits:

Figure 3 caption:

*"**Figure 3** A summary of simulated cloud microphysics on May 11, 13:37 EET during the BAECC campaign. Simulations are performed both with and without organic condensation (red and blue lines, respectively) for three different updraft velocities (see line styles from panel **a**). The initial temperature is 279 K, pressure 980 hPa, and RH is 90%. (**a**) The concentration of SVOCs and IVOCs in the gas phase as a function of distance from cloud base (CB). SVOCs have $\log_{10}C^*$ = [0, 2] and IVOCs $\log_{10}C^*$ = [3, 7] under 279 K.* ***(b) The relative change in critical supersaturation (s*) between noCC and CC simulations, as a function of soluble mass added along the ascent by condensing organics in the simulations, where co-condensation is enabled. The data are shown for a particle with a dry diameter of 147 nm at PARSEC-UFO initialization. The markers represent the relative reductions in s^* (between CC and noCC) at the time when maximum supersaturation (s_{max}) was reached. (c–d)*** *The evolution of the s_{max} and CDNC with altitude, respectively. (**e**) The droplet spectra 50 meters above CB. Size bins exceeding the critical diameter as predicted by Köhler theory are calculated as cloud droplets. The red lines are obtained with F volatility distributions (**Fig. 2a**). The line type specifications in panels **d–e** follow those shown in panel **a** and the colors used in panels **d–e** are documented in the panel **c** legend."*

References

Aalto, P., Hämeri, K., Becker, E., Weber, R., Salm, J., Mäkelä, J. M., Hoell, C., O'dowd, C. D., Hansson, H.-C., Väkevä, M., Koponen, I. K., Buzorius, G., and Kulmala, M.: Physical characterization of aerosol particles during nucleation events, Tellus B: Chemical and Physical Meteorology, 53, 344–358, https://doi.org/10.3402/tellusb.v53i4.17127, 2001.

Äijälä, M., Heikkinen, L., Fröhlich, R., Canonaco, F., Prévôt, A. S. H., Junninen, H., Petäjä, T., Kulmala, M., Worsnop, D., and Ehn, M.: Resolving anthropogenic aerosol pollution types – deconvolution and exploratory classification of pollution events, Atmospheric Chemistry and Physics, 17, 3165–3197, https://doi.org/10.5194/acp-17-3165-2017, 2017.

ARM Data Center: Atmospheric Radiation Measurement (ARM) user facility. 2014, updated hourly. Interpolated Sonde (INTERPOLATEDSONDE). 2014-04-01 to 2014-07-01, ARM Mobile Facility (TMP) U. of Helsinki Research Station (SMEAR II), Hyytiala, Finland; AMF2 (M1). Compiled by M. Jensen, S. Giangrande, T. Fairless and A. Zhou., 2014.

Crooks, M., Connolly, P., Topping, D., and McFiggans, G.: Equilibrium absorptive partitioning theory between multiple aerosol particle modes, Geosci. Model Dev., 9, 3617–3637, https://doi.org/10.5194/gmd-9-3617-2016, 2016.

Crooks, M., Connolly, P., and McFiggans, G.: A parameterisation for the co-condensation of semi-volatile organics into multiple aerosol particle modes, Geosci. Model Dev., 11, 3261–3278, https://doi.org/10.5194/gmd-11-3261-2018, 2018.

Gysel, M., Crosier, J., Topping, D. O., Whitehead, J. D., Bower, K. N., Cubison, M. J., Williams, P. I., Flynn, M. J., McFiggans, G. B., and Coe, H.: Closure study between chemical composition and hygroscopic growth of aerosol particles during TORCH2, Atmos. Chem. Phys., 7, 6131–6144, https://doi.org/10.5194/acp-7-6131-2007, 2007.

Heikkinen, L., Äijälä, M., Riva, M., Luoma, K., Daellenbach, K., Aalto, J., Aalto, P., Aliaga, D., Aurela, M., Keskinen, H., Makkonen, U., Rantala, P., Kulmala, M., Petäjä, T., Worsnop, D., and Ehn, M.: Long-term sub-micrometer aerosol chemical composition in the boreal forest: inter- and intra-annual variability, Atmos. Chem. Phys., 20, 3151–3180, https://doi.org/10.5194/acp-20-3151-2020, 2020.

Hussein, T., Maso, M. D., Petäjä, T., Koponen, I. K., Paatero, P., Aalto, P. P., Hämeri, K., and Kulmala, M.: Evaluation of an automatic algorithm for fitting the particle number size distributions, Boreal Environ. Res., 10, 19, 2005.

Luoma, K.: AEROSOL OPTICAL PROPERTIES, BLACK CARBON AND THEIR SPATIO-TEMPORAL VARIATION, PhD thesis, University of Helsinki, 2021.

Petters, M. D. and Kreidenweis, S. M.: A single parameter representation of hygroscopic growth and cloud condensation nucleus activity – Part 2: Including solubility, Atmos. Chem. Phys., 7, 2008.

Sihto, S.-L., Mikkilä, J., Vanhanen, J., Ehn, M., Liao, L., Lehtipalo, K., Aalto, P. P., Duplissy, J., Petäjä, T., Kerminen, V.-M., Boy, M., and Kulmala, M.: Seasonal variation of CCN concentrations and aerosol activation properties in boreal forest, Atmospheric Chemistry and Physics, 11, 13269–13285, https://doi.org/10.5194/acp-11-13269-2011, 2011.